Supplementary Materials for

Organometallic and radical intermediates reveal mechanism of diphthamide biosynthesis

Min Dong, Venkatesan Kathiresan, Michael K. Fenwick, Andrew T. Torelli, Yang Zhang, Jonathan D. Caranto, Boris Dzikovski, Ajay Sharma, Kyle M. Lancaster, Jack H. Freed, Steven E. Ealick,* Brian M. Hoffman,* Hening Lin*

*Corresponding author. Email: see3@cornell.edu (S.E.E.); bmh@northwestern.edu (B.M.H.); hl379@cornell.edu (H.L.)

Published 16 March 2018, *Science* **359**, 1247 (2018)
DOI: 10.1126/aao6595

This PDF file includes:

Materials and Methods

Materials

The plasmid containing the human methionine adenosyltransferase I (MATI) gene was a generous gift from Dr. Minkui Luo (Memorial Sloan–Kettering Cancer Center). SAM was purchased from Santa Cruz Biotechnology, Inc. and neutralized to pH 7.4 before use. Ammonium-$^{15}N_2$ sulfate, $^{13}C_5$-*L*-methionine, $^{2}H_5$-*L*-histidine and $^{13}C_5$-*L*-histidine were purchased from Cambridge Isotope Laboratories, Inc. ^{57}Fe powder was purchased from Isoflex USA.

Expression and purification of yeast Dph1-Dph2

Dph1-Dph2 plasmid was co-transformed with pDB1282 (*15*), which contains the *Azotobacter vinelandii* ISC operon to increase the iron sulfur cluster loading, in BL21 (DE3) pRARE2 strain. Dph1-Dph2 protein was expressed and purified following previously reported protocol (*6*) with slight modifications.

Cells were grown in 2 liters LB medium with 100 μg/ml ampicillin, 20 μg/mL chloramphenicol and 50 μg/mL kanamycin at 37 ℃ and 200 rpm. At optical density (OD_{600}) of 0.3, solid arabinose was added to each flask at a final concentration of 0.1 % (w/v). When the OD_{600} reached to 0.6, the cultures were cooled down in a ice-water bath and supplemented with $FeCl_3$, $Fe(NH_4)_2(SO_4)_2$ and L-cysteine to final concentrations of 50 μM, 50 μM and 400 μM, respectively. Protein expression was induced by 0.1 mM isopropyl-β-D-thiogalactopyranoside (IPTG), at which point the culture flasks were sealed to limit the amount of oxygen in the system. Cells were incubated in a shaker at 18 ℃ and 200 rpm for 20 h before harvested.

Purification of Dph1-Dph2 was performed in a Coy anaerobic chamber. Cell pellet from 2 liter culture was suspended in 40 mL lysis buffer (500 mM NaCl, 10 mM $MgCl_2$, 5 mM imidazole, 1 mM DTT, and 200 mM Tris-HCl at pH 7.4). Lysozyme (200mg) and nuclease (4 μL, 25 U/ml of lysis buffer, Thermo) were added and incubated at 25 °C for 1 h. The mixture was then frozen with liquid nitrogen and then thawed at 25 °C twice. Cell debris was removed by centrifugation at 20,000g (Beckman Coulter Avanti J-E) for 30 min. The supernatant was incubated for 0.5 h with 1.2 ml Ni-NTA resin (Qiagen) pre-equilibrated with the lysis buffer. The Ni-NTA resin was loaded onto a polypropylene column and washed with 20 ml lysis buffer, followed by 20 ml of 30 mM imidazole in lysis buffer. Dph1-Dph2 was eluted from the column with elution buffers (100 mM, 150 mM and 200 mM imidazole in the lysis buffer, 1.5 mL each). The brown-colored elution fractions were buffer-exchanged to 150 mM NaCl, 1 mM DTT and 200 mM Tris-HCl at pH 7.4 and 5% glycerol using a Bio-Rad 10-DG desalting column. The purified proteins were concentrated using Amicon Ultra-4 centrifugal filter devices (Millipore). Protein concentration was determined by Bradford assay. Iron content of the protein was analyzed using an iron assay kit (Bioassay Systems). Sulfur content was analyzed using a reported procedure (*16*). The as isolated Dph1-Dph2 heterodimer usually has 30~50% cluster loading (Taking the assumption that Dph1 and Dph2 each unite bounds a 4Fe-4S cluster based on the structure of *Ph*Dph2 homodimer). The iron and sulfur contents could be increased to 8.0 and 7.9 per Dph1-Dph2 heterodimer (~100% cluster loading) by using in vitro reconstitution method, but there was no obvious increase in the catalytic activity of the protein. Therefore, the following experiments were all performed with the as isolated Dph1-Dph2.

^{57}Fe enriched Dph1-Dph2 was prepared similarly but in M9 minimal medium supplemented with 0.2% (w/v) glucose, 2 mM $MgSO_4$ and 0.1 mM $CaCl_2$. ^{57}Fe powder was dissolved in 2 M HCl with pH adjusted to 5~6 as a stock solution. The ^{57}Fe stock solution and L-cysteine were added to M9 media to final concentrations of 100 μM and 400 μM, respectively.

Expression and purification of wild type EF2, EF2 H699A mutant, ^{2}H-His, ^{13}C-His and ^{15}N-His labeled EF2

The *Saccharomyces cerevisiae* EF2 wild type and H699A mutant were expressed and purified essentially as described before (*17*) with the following modification. After harvesting and resuspending the cells in 20 mM Tris-HCl buffer (pH 8.0) containing 400 mM $(NH_4)_2SO_4$, 10 mM $MgCl_2$, and 1 mM protease inhibitor PMSF, cells were lysed using glass beads with a bead beater (Biospec).

For expression of $^{2}H_5$-His and ^{13}C-His labeled EF2, the EF2 gene was cloned into p426MET25 vector (ATCC, Manassas, VA) as described before using the same restriction sites (*18*). The plasmid was transformed into ⊿*dph2 S. cerevisiae* strains with BY4741 background (OpenBiosystems, Huntsville, AL). To express the isotope labeled EF-2 proteins, the transformed cells were grown in synthetic complete media with $^{2}H_5$-histidine or $^{13}C_5$-histidine replacing normal histidine and lacking uracil for 48 hours.

The ^{15}N-His EF2 protein was expressed using a strain containing plasmid p423 MET25-EF2 (*17*). The cells were grown in synthetic complete media lacking histidine, with ammonium-$^{15}N_2$ sulfate replacing the ammonium-$^{14}N_2$ sulfate.

The fermentation service was provided by Bioexpression and Fermentation Facility at University of Georgia. Aerobically purified all EF2 proteins were degassed by Schlenk line before use.

Expression and purification of human methionine adenosyltransferase I (MATI)

The pNIC28-Bsa4 vector containing the MATI gene was used to transform BL21(DE3) pRARE2 strain. N-terminal 6×His MATI was expressed and purified following reported procedures (*19*).

Production of (methionine-$^{13}C_5$)-SAM

(Methionine-$^{13}C_5$)-SAM was synthesized in a 1 mL reaction containing 50 mM Tris–HCl (pH 8.0), 100 mM KCl, 2 mM $MgCl_2$, 10 mM ATP, 30 μM MATI, and 5 mM $^{13}C_5$-methionine. The reaction mixture was incubated at room temperature (23 ℃) for 12 hr before being quenched with 1 mL of 10% trifluoroacetic acid (TFA) aqueous solution. After centrifugation at 14,000 g for 20 min, the supernatant was purified by reverse-phase HPLC. (Methionine-$^{13}C_5$)-SAM was eluted at 11 min with a flow rate of 8 mL/min with 0.1% TFA as mobile phases. LCMS (ESI) calcd. for $C_{10}{}^{13}C_5H_{23}N_6O_5S$ $[M]^+$ 404.2, obsd. 404.0.

Rapid Freeze Quench (RFQ) sample preparation for EPR/ENDOR spectroscopy

RFQ experiments were performed with a Bio-Logic SFM300 with two glass syringes. O_2 was removed from mixing lines and anaerobic samples were loaded into the system as previously described for the Bio-Logic stopped-flow SFM300 configuration

(*20*). Sample syringes were filled and capped in an anaerobic glove box. One syringe was filled with 400 μM Dph1-Dph2 and 260 μM SAM with or without 260 μM EF2 in 200 mM Tris-HCl, pH 7.4, and 150 mM NaCl. Another syringe was filled with 20 mM dithionite in 200 mM Tris-HCl, pH 7.4, and 150 mM NaCl. The solutions were loaded into the RFQ and mixed at 1:1(v/v) ratio (190 μl total per sample) and collected at selected time points. The reaction mixture was injected into a funnel coupled to an EPR or ENDOR tube and filled with liquid ethane (~-170 ℃). The frozen samples were packed using a stainless steel rod. The tubes were stored in liquid nitrogen tank before spectroscopic characterization.

The 2 min time point samples for isotope EPR study of the organic radical on EF2 were hand quenched in an anaerobic chamber. The reaction contained 400 μM Dph1-Dph2, 1 mM SAM or (methionine-$^{13}C_5$)-SAM, and 260 μM EF2 or $^{2}H_5$-His labeled EF2 in 200 mM Tris-HCl, pH 7.4, and 150 mM NaCl. Upon adding dithionite in the reaction to a final concentration of 10 mM, samples were immediately transferred to EPR tubes and quenched by freezing in liquid nitrogen at 2 min.

EPR and ENDOR measurements

X band EPR spectra were recorded on a Bruker ElexSys E500 EPR spectrometer at a frequency of 9.38 GHz. EPR measurements at 12 K, 35 K and 70 K were carried out using an ESR 910 liquid-helium cryostat (Oxford Instruments). The spectrometer settings were as follows: modulation frequency, 100 kHz; modulation amplitude, 8 G; microwave power, 0.63 mW. The field sweeps were calibrated with a Bruker ER 035 Gauss meter and the microwave frequency was monitored with a frequency counter. Data acquisition and manipulation were performed with Xepr software. ENDOR spectra were collected on a spectrometer with a helium immersion dewar as previously reported (*21, 22*). ENDOR measurements were done at 2 K.

EPR integrations and simulations were performed with the SpinCount program developed by Dr. Michael P. Hendrich.

Time course experiment for the quantification of ACP modified EF2 by Mass-Spec

The reaction mixture was assembled in an anaerobic chamber. The reaction contained 200 μM Dph1-Dph2, 130 μM SAM, and 130 μM EF2 in a buffer of 150 mM NaCl and 200 mM Tris-HCl at pH 7.4 for a total volume of 10 μL. Dithionite (final concentration 10 mM) was injected into the reaction vial to start the reaction. 1 μL aliquot of the reaction was taken out of the vial and quenched with 14 μL of protein loading buffer at different time points: 10 s, 1 min, 2 min, 5 min, 10 min, 30 min, and 40 min. The aliquots in protein loading buffer were taken outside the chamber, subsequently heated at 95 °C for 5 min and then resolved by 12% SDS–polyacrylamide gel electrophoresis. Bands corresponding to EF2 were cut, applied to in-gel digestion and mass-spec analysis.

Preparation of *Ph*Dph2 for Crystallography

A previously described protocol was used to produce protein for the *Ph*Dph2/MTA complex (*5*). The protein used for the *Ph*Dph2/SAM structure was produced with a slightly modified protocol described below. The BL21pRARE *E. coli* expression strain was transformed with the vector containing the *dph2* gene from *P. horikoshii* with an N-

terminal hexahistidine affinity tag. The cells were grown at 37 ℃ and 200 rpm in baffled shaker flasks containing 1.5 L lysogeny broth supplemented with 0.035 g/L chloramphenicol and 0.1 g/L ampicillin. When the cultures reached an optical density (OD) measured at 600 nm of 0.6, $FeCl_3$, $Fe(NH_4)_2(SO_4)_2$ and L-cysteine were added to final concentrations of 50 μM, 50 μM and 400 μM, respectively. Expression was induced with 0.1 mM isopropyl-β-D-thiogalactopyranoside (IPTG) when the culture OD_{600} reached 0.8. After 1.5 h, the incubator temperature and rotation rate were reduced to 15 ℃ and 100 rpm, respectively, and the cultures were allowed to grow for an additional 10-12 h. The cells were harvested by centrifugation at 10,000 *g* for 20 min and the cell paste was flash frozen in liquid nitrogen before storage at -80 ℃.

Frozen cell paste from the equivalent of 4 L of bacterial culture was transferred into a Coy anaerobic chamber and resuspended in 70 mL degassed lysis buffer comprising 0.02 M Tris buffer pH 8.0, 0.5 M NaCl, 0.01 M $MgCl_2$, 0.055 M imidazole (stock pH 8.0), 1 g/L lysozyme, 500 units benzonase (Sigma-Aldrich) and two EDTA-free complete mini protease inhibitor cocktail tablets (Roche). The resuspension was stirred for 45 min at 26 ℃ and then sonicated. The lysate was sealed in centrifuge tubes and centrifuged for 45 min at 39,000 *g* outside the anaerobic chamber and then transferred back into the chamber. The supernatant was decanted to fresh centrifuge tubes, sealed and placed in a 95 ℃ water bath for 10 min to precipitate contaminating proteins. The sample was centrifuged a second time at 39,000 *g* for 30 min and returned to the anaerobic chamber. The supernatant was filtered through a 0.2 μm syringe filter before loading onto a 5 mL HisTrap column (GE Healthcare) equilibrated with binding buffer (same as lysis buffer, without the enzymes or protease inhibitors). The bound protein was washed with 25 mL binding buffer supplemented with a final concentration of 0.08 M imidazole and eluted with a stepwise gradient of imidazole. The peak fraction was dark brown in color and eluted with a buffer containing 0.16 M imidazole. Fractions were combined after analysis by SDS-PAGE and concentrated to a volume of less than 1 mL. The protein was exchanged into a crystallization buffer comprising 0.01 M Tris buffer pH 8.0 and 0.135 M NaCl using a 10DG desalting column (Bio-Rad) prior to crystallization setups.

Crystallization of *Ph*Dph2 complexes

The *Ph*Dph2 in the crystallization buffer was concentrated further in Amicon Ultra 0.5 mL centrifugal concentrators with a 10 kDa MWCO (Millipore Corp.) to a final concentration between 15 and 20 mg/mL measured on a NanoDrop (Thermo Scientific) at 280 nm. SAM was dissolved to a final concentration of 0.2 M in 0.1 M MES buffer pH 6.5, and was added to the concentrated *Ph*Dph2 protein slowly over > 1 min with mixing to a final concentration of 5 mM. All samples were centrifuged at 14,000 *g* for 10 min prior to crystallization. Crystallization experiments were set up in the anaerobic chamber by combining 1.5 μL protein solution with an equal volume of crystallization solution containing 31-35% (v/v) PEG 400, either 0.1 M sodium citrate buffer pH 5.5 or MES buffer pH 6.5, 0.2 M Li_2SO_4 and 2% (v/v) ethylene glycol. These drops were set up in hanging drop format equilibrated over a reservoir of 0.6 M LiCl. The crystals appeared after ~1 week and typically reached sizes of ~200 μm on an edge. Crystals grown from *Ph*Dph2/SAM were cryoprotected by serial transfers in crystallization solution supplemented with decreasing concentrations of Li_2SO_4, increasing concentrations of SAM (10 mM maximum concentration) and increasing concentrations of PEG 400 and

ethylene glycol (25% (v/v) and 5% (v/v), respectively). In the case of MTA, apo crystals prepared without added ligand were serially transferred into solutions matched to the crystallization conditions and increasingly supplemented with PEG400 (32% (v/v) final), ethylene glycol (7.5% (v/v) final), sodium sulfide (0.25 mM final), ferrous ammonium sulfate (0.25 mM final), DTT (5 mM final) and MTA (2.5 mM final). All crystals were cryocooled in the anaerobic chamber by plunging into liquid nitrogen prior to data collection.

X-ray Data Collection and Structure Determination for *Ph*Dph2 complexes.

X-ray diffraction data were collected at Northeastern Collaborative Access Team (NE-CAT) beamline 24-ID-C at the Advanced Photon Source (APS). Diffraction images were collected at crystal to detector distances ranging from 300-350 mm for a total of 100-120 ° of rotation with 1 ° oscillation per image and 1 s exposure to X-rays with wavelengths listed in Table S1. The HKL2000 suite of programs (*23*) was used to index, integrate, scale and merge the diffraction data resulting in statistics that are summarized in Table S1.

Phases for initial models of the structures reported here were obtained using a previous model of *Ph*Dph2 (PDB ID 3LZD) (*5*). PHENIX was used to perform rigid body refinement followed by iterative cycles of all atom positional and ADP refinement with manual model adjustments implemented using COOT (*24, 25*). TLS parameters identified by the TLSMD server (*26*) were included in the refinement as implemented in PHENIX. The quality of the model was monitored throughout refinement using the MOLPROBITY server and as a final model validation criteria (*27*). Refinement statistics are summarized in Table S1.

Crystals of *Ph*Dph2 showed significant anisotropic diffraction resulting in low completeness for the highest resolution data and higher than expected Wilson B-values (Table S1). Both structures also showed large average refined B-factors, and larger than expected differences between Rwork and Rfree.

Preparation of *Cmn*Dph2 for Crystallography

*Cmn*Dph2 was overexpressed and purified using a variation of the protocols used recently to produce other radical SAM enzymes (*28-30*). A codon-optimized *Cmn*Dph2 gene was subcloned from pETDUET-1 into pET-28 using NdeI and XhoI restriction sites for expression of the product NH_2-MGSSHHHHHHSSGLVPRGSHMSE$_2$…Q$_{323}$-COOH. *E. coli* NiCo21(DE3) cells containing plasmid pSuf (*31, 32*) were transformed with pET-28/*Cmn*Dph2 and plated on LB/kanamycin/chloramphenicol agar plates. Cultures were grown in 1.8 L of minimal medium (1 X minimal medium salts, 40 mg/L kanamycin, 34 mg/L chloramphenicol, 4 g/L dextrose, 2 mM $MgSO_4$, and 0.1 mM $CaCl_2$) and shaken at 180 rpm and 37 ℃ until the OD_{600} reached 0.5-0.6 and then chilled in a 4 ℃ cold room for 2.5 h. The cultures were supplemented with L-Cys, $Fe(NH_4)_2(SO_4)_2$, and IPTG at final concentrations of 0.29 mM, 0.089 mM, and 0.18 mM, respectively, and shaken at 50 rpm and 15 ℃ for 20 h. The cultures were chilled in a 4 ℃ cold room, centrifuged at 6,000 g and 4 ℃ for 15 min, and flash frozen in liquid nitrogen. Cell pellets were thawed in a PVC anaerobic chamber (Coy Laboratory Products), suspended in lysis buffer (20 mM Tris-HCl, 500 mM NaCl, and 23 mM imidazole, pH 7.5) supplemented with 5 mM DTT, 0.4 mg/mL lysozyme, and 1.9 kU benzonase, and lysed further on ice via

sonication. The lysate was centrifuged outside the glove box at 60,000 g and 4 ℃ for 20 min and then moved back into the glove box where the supernatant was subjected to immobilized nickel affinity chromatography using lysis and elution (20 mM Tris-HCl, 500 mM NaCl, and 250 mM imidazole, pH 7.5) buffers. The eluate was buffer exchanged into fusion tag cleavage buffer (20 mM HEPES and 200 mM NaCl, pH 7.5) using a Bio-Rad Econo-Pac 10DG desalting column and incubated for 7 h with bovine thrombin (Sigma). The reaction mixture was subjected to subtractive immobilized nickel and benzamidine affinity chromatography, buffer exchanged into 5 mM HEPES and 25 mM NaCl, pH 7.0, and flash-frozen in liquid nitrogen.

Crystallization of *Cmn*Dph2 complexes.

*Cmn*Dph2 was cocrystallized with SAM (Cayman Chemical Company) or SAH using the hanging drop vapor diffusion method at room temperature inside the anaerobic chamber. Drops were prepared with a 1:1 ratio of protein to reservoir solution. The concentration of *Cmn*Dph2 was approximately 0.4 mM and the concentrations of SAM and SAH were 4 mM and 6 mM, respectively. For co-crystallizations with SAM, only reservoir solutions yielding crystals within 20 hours were pursued and the crystals obtained by the end of this time period were cryo-cooled without delay in liquid nitrogen inside the anaerobic chamber. These reservoir solutions contained either 65 mM HEPES, pH 6.5-7.0, and 18-25% (w/v) polyethylene glycol (PEG) 1000 or 100 mM imidazole, pH 6.0-7.0, 15-20 % (w/v) PEG 4000, and 0 or 3 % 2-methyl-2,4-pentanediol. Reservoir solutions for cocrystallizations with SAH were 100 mM HEPES, pH 6.0-6.5, 200 mM ammonium chloride, and 16-20% (w/v) PEG 4000. PEG concentrations were increased 10-25% in the cryoprotectant.

X-ray Data Collection and Structure Determination for *Cmn*Dph2 complexes.

X-ray diffraction experiments were performed at beamlines NE-CAT 24-ID-C or 24-ID-E of the APS. *Cmn*Dph2 crystals were irradiated with X-rays having wavelengths λ = 0.9792 or 0.9791 Å at 100 K. X-ray diffraction images were recorded for 1 °s oscillations using a PILATUS 6MF detector located 460 mm from a *Cmn*Dph2/SAM crystal and 318 mm from a *Cmn*Dph2/SAH crystal and on a EIGER X 16M detector located 300 mm from a *Cmn*Dph2/SAM crystal. Images were processed using HKL2000 (*23*) (Table S1). The structure of *Cmn*Dph2 was determined via molecular replacement using Phaser within PHENIX (*24*, *33*) with the structure of *Ph*Dph2 (*5*) used as a search model. Automated structure refinement was performed using PHENIX (*24*) and manual model building was performed using COOT (*25*) (Table S1).

Crystals of *Cmn*Dph2 complexed with SAM showed a mixture of cleaved and uncleaved SAM resulting in slightly higher than expected differences between Rwork and Rfree (Table S1). *Cmn*Dph2/SAM1 showed less cleaved SAM and refined better compared to *Cmn*Dph2/SAM2, which showed approximately equal amounts of cleaved and uncleaved SAM. Crystals of *Cmn*Dph2 also showed translational pseudosymmetry, however, this did not appear to affect the refinement because*Cmn*Dph2/SAH, for which the ligand is expected to be uncleaved, showed normal refinement statistics.

Supplementary Text

Fig. S3 shows that the structure of intermediate II parallels those recently found for the substrate radical intermediate of the antibiotic resistance protein, Cfr (*34*) and for the cross-linked protein-nucleic acid radical formed in the reaction catalyzed by the RS enzyme, RlmN (*35*).

Fig. S4A shows the intermediate II EPR spectrum and simulations with the large ^{1}H and ^{14}N hyperfine couplings whose tensor values are given in the figure legend. As shown in this panel, the broad component lines of the ^{1}H doublet incorporate the ^{14}N features, unlike the case of Cfr (*34*) and RlmN (*35*), where subtle shoulders indicate the presence of this interaction. To place an upper bound on the ^{14}N A3 tensor component, simulations were performed as this value was progressively increased. As illustrated in **Fig. S4B**, such shoulders appear in the simulation by A3 =70 MHz, yielding as an upper bound A3 $\lesssim$ 65 MHz.

Fig. S5 shows field-modulated ^{13}C and ^{15}N 35 GHz CW ENDOR spectrum of intermediate II freeze-trapped in a reaction containing EF2 with ^{13}C labeling or uniform ^{15}N labeling of His (^{13}C-His, ^{15}N-His EF2), where ^{13}C hyperfine couplings to two His carbons, with $A_{iso} \approx$ 7.5 and 4.2 MHz or ^{15}N features over the range of 6-16 MHz (Fig. S4) were observed. The ^{13}C-His EF2 sample also showed broadening of the EPR spectrum in comparison with natural-abundance EF2 (Fig. S6).

Fig. S7 shows kinetic competence of intermediate I and II. The spin quantities of intermediates I and II were determined from EPR time points by integration or simulation using SpinCount. Due to the saturation issue of the EPR signals, an accurate quantification was excluded. Instead, relative amounts of intermediate I and II in each time points were calculated from the relative intensities of the EPR signals to the detected maximum signals (2 s for intermediate I and 2 min for intermediate II). EPR spectra at 35 K were used for intermediate I quantification, while the 70 K spectra were used for intermediate II quantification. In parallel, the accumulation of ACP modified EF2 was quantified at several time points by mass spectrometer. Observed rate constants (k_{obs}) are resulted from fitting single or double exponent equations to the time courses. The k_{obs} for intermediate I decay ($k_{obs(decay)}$) is equivalent to the k_{obs} for intermediate II formation ($k_{obs(formation)}$) within the fitting error. Similarly, $k_{obs(decay)}$ for intermediate II is equal to the $k_{obs(formation)}$ for modified EF2. Importantly, $k_{obs(formation)}$ of intermediate I> $k_{obs(decay)}$ of intermediate I/$k_{obs(formation)}$ of intermediate II > $k_{obs(decay)}$ of intermediate II/$k_{obs(formation)}$ of modified EF2, which is consistent with intermediates I and II being kinetically competent for the first step of diphthamide biosynthesis by the mechanism proposed in Fig. 4.

Additional archaeal Dph2 crystal structures.

We first obtained the structure of *Ph*Dph2 in complex with SAM. While SAM could be modeled into the difference electron density for the *Ph*Dph2/SAM complex (Fig. S8), the fit was not ideal and was different for the two subunits. Further analysis suggested that a better fit might be obtained using a mixture of SAM, and the cleavage products MTA and 2-aminobutyrate (2AB). We then prepared crystals of *Cmn*Dph2 in the presence of SAM. While these crystals diffracted to slightly higher resolution, the results were similar to *Ph*Dph2, also suggesting a mixture of SAM and cleavage products (Fig. S9). The structure suggests that prior to SAM cleavage, both the amino and carboxylate groups are coordinated to the differentiated iron, and that after cleavage of SAM, the resulting 2AB shifts slightly to a new position in which only the amino group is coordinated to iron and the carboxylate group is hydrogen bonded to the amide of Gly158, the side chain of His180, and the side chain of Arg285. We then prepared high resolution crystals of *Cmn*Dph2 with the SAM analogue S-adenosylhomocysteine (SAH). In this case, the SAH electron density was clear and continuous in both subunits, and showed a similar geometry for the aminocarboxypropyl group atoms compared to the *Cmn*Dph2/SAM complex, with Cγ closest to, and the amino and carboxylate groups coordinated to, the differentiated iron of the cluster (Fig. S10). The model of the *Cmn*Dph2/SAM complex is also consistent with the structure of *Ph*Dph2 in complex with SAM or the cleaved product. Finally, *Cmn*Dph2 was crystallized with SAM using a procedure to minimize the SAM cleavage reaction (see methods). The resulting electron density showed clear evidence for SAM with only minimal cleavage (Fig. S11, Fig 3) and with both the amino and carboxylate groups coordinated to the differentiated iron.

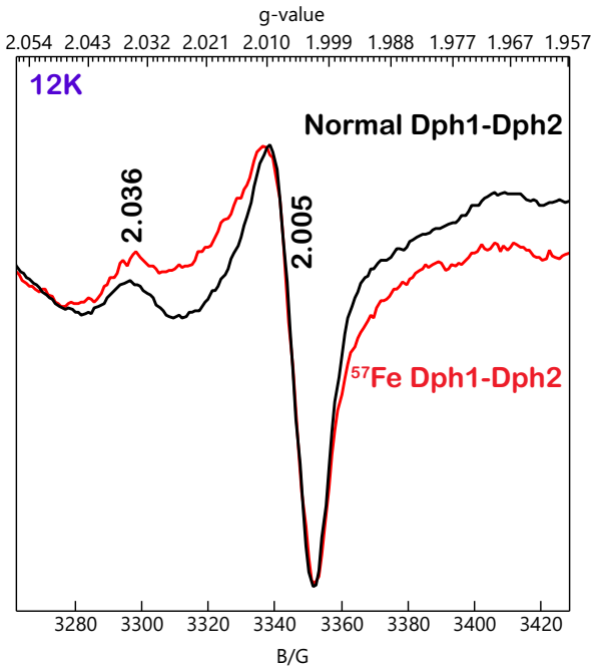

Fig. S1. X-band EPR spectra of Intermediate I quenched at 2 s, (Black) Normal Dph1-Dph2; (Red) ^{57}Fe-Enriched Dph1-Dph2, which adds 4 gauss to the linewidth. *Conditions:* Modulation amplitude, 8 G; T = 12 K

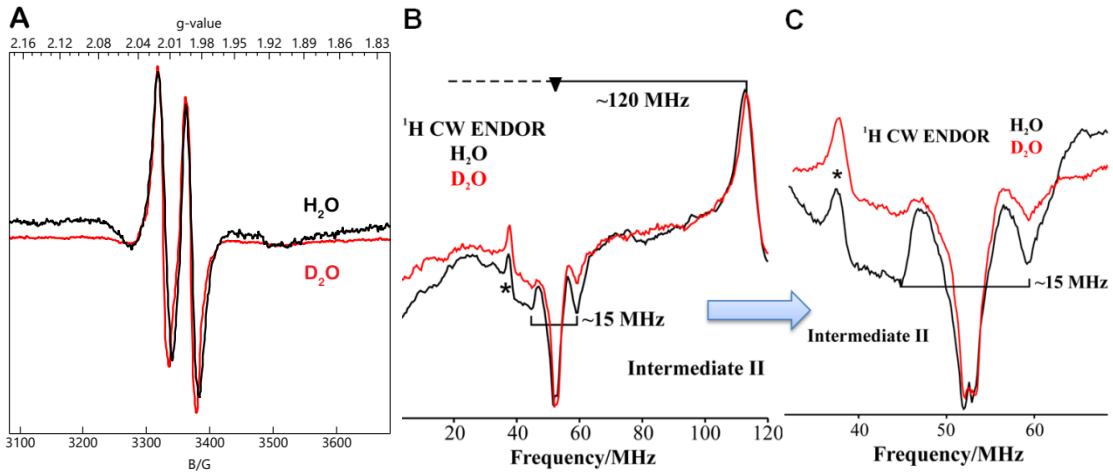

Fig. S2. (A) X-band CW EPR of Intermediate II prepared in H_2O and D_2O, showing only slight narrowing of the non-exchangeable doublet in D_2O. (B, C) Q-band CW ^{1}H-ENDOR spectrum for intermediate II prepared in H_2O and D_2O (quenched at 2 min). Braces indicate hyperfine splittings; (*) is third harmonic of ^{1}H peak at ~ 115 MHz. The large hyperfine splitting (A ≈ 120 MHz) is from a non-exchangeable proton. A moderate coupling (A ~ 15 MHz) that is exchangeable is visible in both spectra. *EPR Conditions:* T=70 K. *ENDOR Conditions: (B)* Microwave Frequency: 34.6869 GHz; Modulation Amplitude: 1.6 G; RF Sweep: 3-120 MHz; RF Sweep Rate: 0.75 MHz/s; Time Constant: 32 ms; Number of Scans: 5; Magnetic Field: 12296 G; Temperature: 2 K. ***(C)*** Same as B, except Microwave Frequency: 34.825 GHz; Magnetic Field: 12344 G.

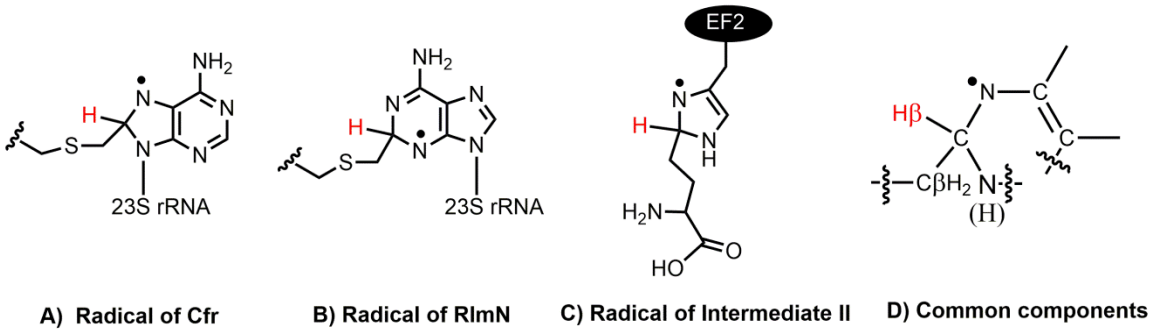

Fig. S3. Structures of the Cfr, RlmN, and intermediate II radicals (A-C), and a cartoon incorporating the common components of three radicals (D).

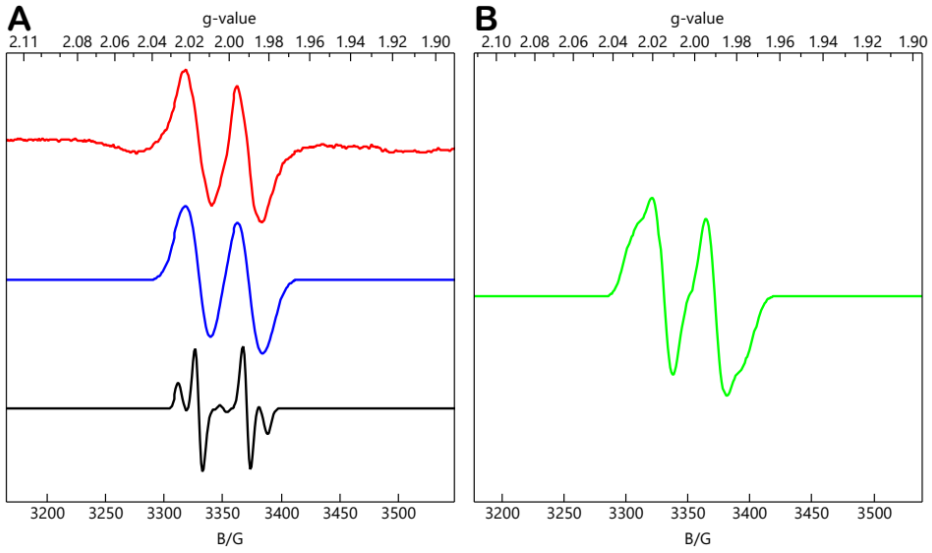

Fig. S4. (A) Simulation of CW EPR spectrum of intermediate II: Experimental (red trace); Simulation with near-isotropic ^{1}H coupling A= 122, 122, 103 MHz and ^{14}N coupling A=4, 4, 54 MHz, linewidth, 8 MHz (blue trace). Simulation with same hyperfine interactions, but with linewidth, 3 MHz (black trace) (B) Simulation of panel A, red trace, with ^{1}H coupling of A= 122, 122, 103 MHz and ^{14}N coupling of A3 = 70 MHz.

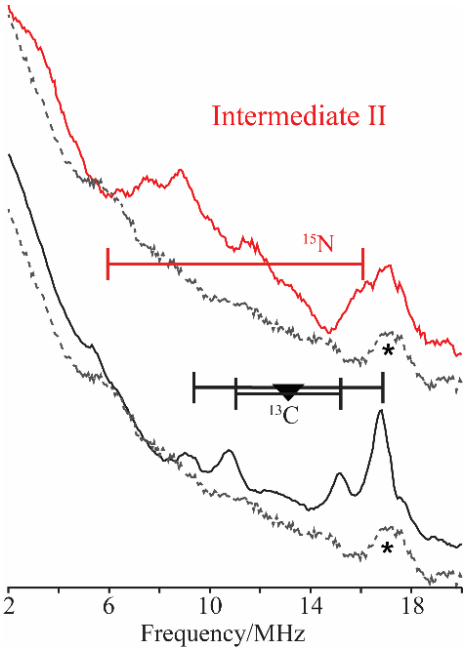

Fig. S5. Q-band CW ENDOR spectra at 2 K for intermediate II prepared with: *Upper* [red], uniform ^{15}N labeling of His-EF2 overlaid with [gray/dashed] natural abundance spectrum; (*) signal at ~17 MHz, 3rd harmonic of ^{1}H signals in vicinity of ^{1}H Larmor frequency; brace indicates range of frequency of ^{15}N signals. *Lower* [black], ^{13}C-His EF2 overlaid with [gray/dashed] natural-abundance EF2. Triangle indicates Larmor frequency of ^{13}C, braces indicate hyperfine splittings, (*) as in *Upper*. *Conditions:* Microwave Frequency: 34.7245 (for upper and lower samples) / 34.788 GHz (for gray/dashed sample); Modulation Amplitude: 1 G; RF Sweep: 2-20 MHz; RF Sweep Rate: 1 MHz/s (for black sample) and 0.5 MHz/s (for both red and gray/dashed samples); Time Constant: 32 ms; Number of Scans: 500 (for black sample, bottom), 154 (for red sample, top), and 200 (for gray/dashed sample); Magnetic Field: 12330 G (for black sample, bottom), 12320 G (for red sample, top), 12335 G (for gray/dashed sample); Temperature: 2 K.

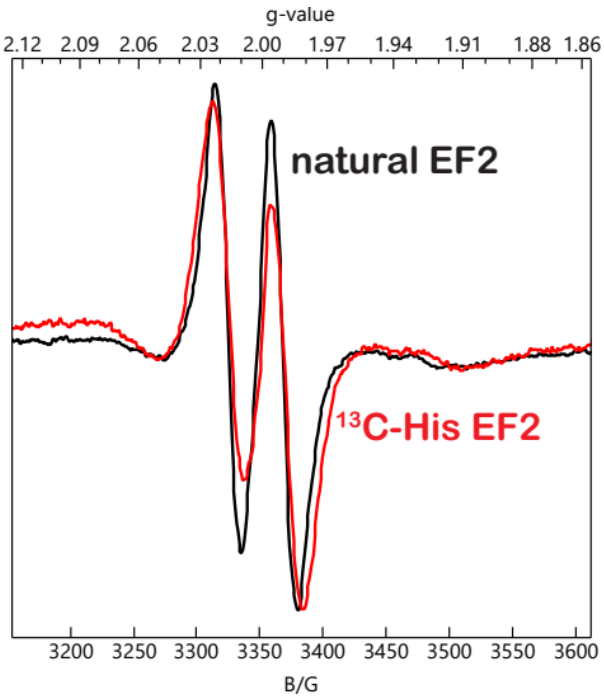

Fig. S6. X-band CW EPR spectra of intermediate II with natural EF2 and ^{13}C-His EF2 at 70K.

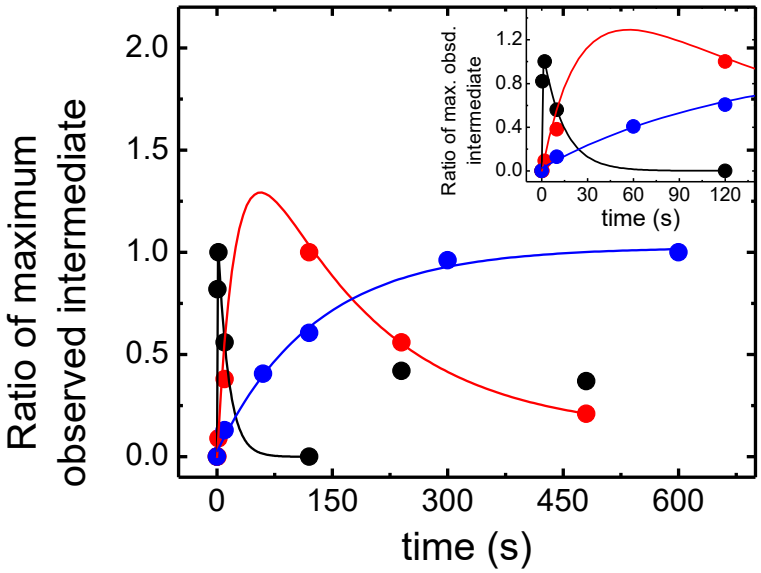

Time course	$k_{obs(formation)}$ (s^{-1})	$k_{obs(decay)}$ (s^{-1})
Intermediate I (Black)	2.699 ±0.002	0.07313 ±0.00005
Intermediate II (Red)	0.040 ±0.009	0.006 ±0.002
EF-2 Modification (Blue)	0.0078 ±0.0008	

Fig. S7. Kinetic competence of intermediate I and II. Time dependence of formation and decay of intermediate I (black) and intermediate II (red) determined by EPR spectra from RFQ samples; ACP modified EF2 formation (blue) determined by mass spectrometer.

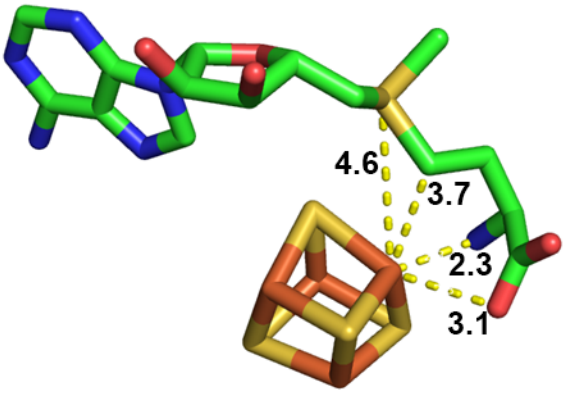

Fig. S8. Cluster and bound SAM in the structure of *Ph*Dph2. Distances are given in angstroms.

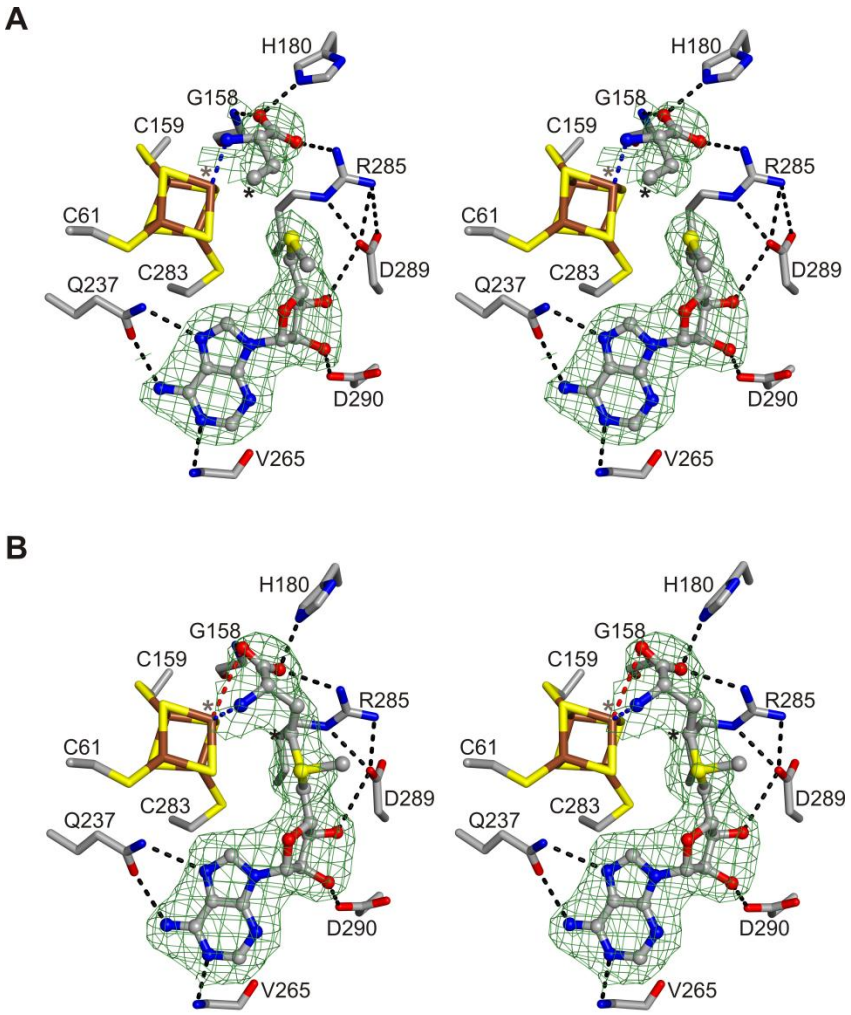

Fig. S9. Structure of *Cmn*Dph2 cocrystallized with SAM. The electron density shows a mixture of SAM and cleavage products. (A) Subunit A contains mostly MTA and 2AB. (B) Subunit B contains mostly uncleaved SAM. A composite omit map was computed using PHENIX and the region around the ligands is shown using a green mesh contoured at 0.3 times the RMS value of the map using PyMOL. The black dashed lines indicate potential hydrogen bonds between active site residues and ligands. The blue and red dashed lines indicate bonds with the differentiated iron of the [4Fe-4S] cluster. The black and brown asterisks label C_γ of SAM and the differentiated iron of the [4Fe-4S] cluster, respectively.

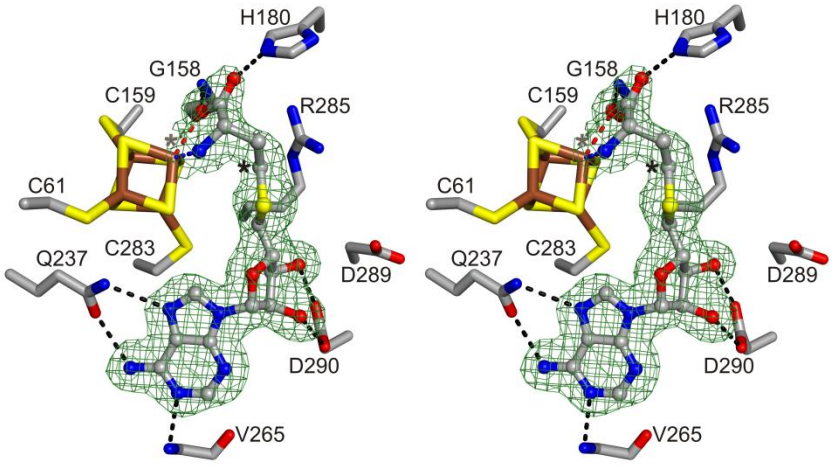

Fig. S10. Structure of *Cmn*Dph2 in complex with SAH. A composite omit map was computed using PHENIX and the region around SAH is shown using a green mesh contoured at 0.5 times the RMS value of the map using PyMOL. The black dashed lines indicate potential hydrogen bonds between SAH and active site residues. The blue and red dashed lines indicate bonds with the differentiated iron of the [4Fe-4S] cluster. The black and brown asterisks label C_γ of SAH and the differentiated iron of the [4Fe-4S] cluster, respectively.

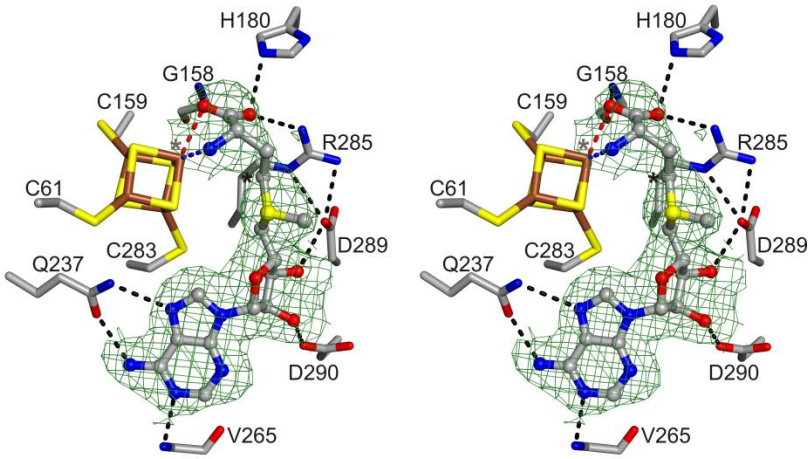

Fig. S11. Structure of *Cmn*Dph2 in complex with uncleaved SAM. A composite omit map was computed using PHENIX and the region around SAM is shown using a green mesh contoured at 0.5 times the RMS value of the map using PyMOL. The black dashed lines indicate potential hydrogen bonds between SAM and active site residues. The blue and red dashed lines indicate bonds with the differentiated iron of the [4Fe-4S] cluster. The black and brown asterisks label C_γ of SAM and the differentiated iron of the [4Fe-4S] cluster, respectively.

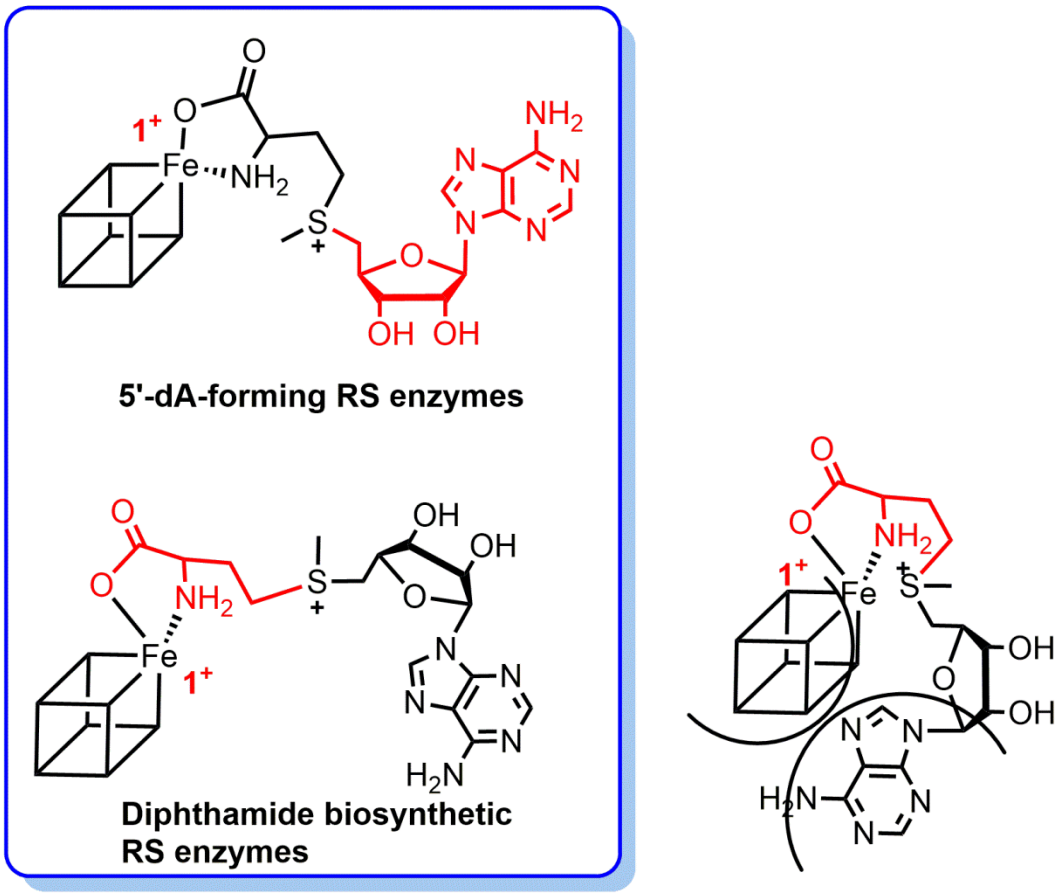

Fig. S12. Regioselectivity control in SAM cleavage by 5′-dA• forming RS enzymes ($C_{5'\text{-}dA}$-S-Fe co-linear) and diphthamide biosynthetic RS enzymes (S-$C_{\gamma,Met}$-Fe co-linear)(blue box, left panel). For the $C_{\gamma,Met}$-S bond cleavage in diphthamide biosynthetic RS enzymes, a radical displacement reaction with $C_{\gamma,Met}$-S-Fe co-linear arrangement (right panel) is unlikely due to the steric hindrance introduced by conformational constraints on SAM.

Table S1. X-ray Diffraction Data Processing and Structure Refinement Statistics[a]

	PhDph2/MTA	PhDph2/SAM	CmnDph2/SAM1	CmnDph2/SAM2	CmnDph2/SAH
data collection					
beamline	APS 24-ID-C	APS 24-ID-C	APS 24-ID-C	APS 24-ID-C	APS 24-ID-C
Wavelength (Å)	0.9792	0.9792	0.9792	0.9792	0.9792
space group	$P2_12_12_1$	$P2_12_12_1$	$P2_12_12_1$	$P2_12_12_1$	$P2_12_12_1$
unit cell dimensions	*a* = 55.5 Å, *b* = 80.5 Å, *c* = 161.9 Å,	*a* = 57.0 Å, *b* = 80.9 Å, *c* = 161.1 Å	*a* = 61.9 Å, *b* = 64.1 Å, *c* = 158.4 Å,	*a* = 31.5 Å, *b* = 127.2 Å, *c* = 142.5 Å,	*a* = 31.4 Å, *b* = 128.0 Å, *c* = 140.9 Å,
resolution[a] (Å)	50.0 – 2.4 (2.43 – 2.35)	50.0 – 2.3 (2.35 – 2.30)	49.8 – 2.3 (2.33 – 2.25)	44.5 – 2.1 (2.15 – 2.08)	47.5 – 1.7 (1.71 – 1.65)
total # reflections	130,240	132,891	138,805	159,054	210,888
# unique reflections	29,510 (2,311)	33,136 (1,946)	30,482 (3,016)	35,318 (3,416)	67,396 (6,516)
R_{merge} (%)[a,b]	6.2 (33.8)	5.5 (36.1)	9.7 (57.9)	9.3 (57.9)	5.3 (55.7)
R_{pim} (%)	3.7 (27.0)	3.5 (25.4)	5.0 (31.5)	4.7 (29.8)	3.4 (35.6)
$I/\sigma(I)$	20.0 (2.7)	20.1 (2.3)	11.2 (1.9)	11.7 (2.5)	16.4 (2.2)
CC1/2	0.997 (0.913)	0.998 (0.929)	0.997 (0.797)	0.997 (0.842)	0.996 (0.755)
completeness (%)	94.8 (75.3)	97.8 (88.1)	99.6 (99.5)	99.0 (98.7)	97.1 (96.5)
multiplicity	4.4 (2.7)	4.0 (4.0)	4.6 (4.3)	4.5 (4.4)	3.1 (3.1)
Wilson B	46.1	53.6	31.0	31.9	24.3
refinement					
resolution (Å)	40.5 – 2.4	46.5 – 2.3	49.8 – 2.3	44.5 – 2.1	47.5 – 1.7
# reflections	29,337	32,972	30,423	34,190	67,303
R_{work}[c]/ R_{free} (%)	18.3/25.0	18.8/24.9	17.5/22.7	20.1/26.0	18.1/21.7
# protein atoms	5,184	5,250	4,793	4,651	5,162
# ligand atoms	66	70	70	70	68
# water atoms	53	69	200	219	305
avg. B-factors (Å^2)					
protein atoms	66.1	68.0	36.4	43.0	39.2
ligand atoms	90.8	79.0	32.0	34.8	28.9
water atoms	54.2	54.0	38.4	44.4	42.2
rmsd for bonds (Å)	0.007	0.007	0.007	0.008	0.008
rmsd for bonds (Å)	0.007	0.007	0.007	0.008	0.008
rmsd for angles (°)	0.847	0.831	0.929	0.926	0.996
Ramachandran analysis (%)					
favored	95.68	96.42	97.12	96.31	96.86
allowed	4.02	3.43	2.72	3.52	3.14
outliers	0.3	0.15	0.16	0.17	0
PDB ID	6BXK	6BXL	6BXM	6BXN	6BXO

[a] Values in parentheses refer to the highest-resolution shell.

[b] $R_{merge} = \Sigma\Sigma_i \mid I_i - \langle I \rangle \mid / \Sigma \langle I \rangle$, where $\langle I \rangle$ is the mean intensity of the N reflections with intensities I_i and common indices h,k,l.

[c] $R_{work} = \Sigma_{hkl} \mid |F_{obs}| - k\,|F_{cal}| \mid / \Sigma_{hkl} |F_{obs}|$ where F_{obs} and F_{cal} are observed and calculated structure factors, respectively, calculated over all reflections used in the refinement. R_{free}, is similar to R_{work} but calculated over a subset of reflections matched to those used for the structure used for Fourier synthesis (PDB ID 3LZC) (*5*) and were excluded from all stages of refinement.

References

1. E. A. Robinson, O. Henriksen, E. S. Maxwell, Elongation factor 2. Amino acid sequence at the site of adenosine diphosphate ribosylation. *J. Biol. Chem.* **249**, 5088–5093 (1974). Medline

2. B. G. Van Ness, J. B. Howard, J. W. Bodley, ADP-ribosylation of elongation factor 2 by diphtheria toxin. Isolation and properties of the novel ribosyl-amino acid and its hydrolysis products. *J. Biol. Chem.* **255**, 10717–10720 (1980).

3. B. G. Van Ness, J. B. Howard, J. W. Bodley, ADP-ribosylation of elongation factor 2 by diphtheria toxin. NMR spectra and proposed structures of ribosyl-diphthamide and its hydrolysis products. *J. Biol. Chem.* **255**, 10710–10716 (1980). Medline

4. R. Schaffrath, W. Abdel-Fattah, R. Klassen, M. J. Stark, The diphthamide modification pathway from *Saccharomyces cerevisiae*—revisited. *Mol. Microbiol.* **94**, 1213–1226 (2014). doi:10.1111/mmi.12845 Medline

5. Y. Zhang, X. Zhu, A. T. Torelli, M. Lee, B. Dzikovski, R. M. Koralewski, E. Wang, J. Freed, C. Krebs, S. E. Ealick, H. Lin, Diphthamide biosynthesis requires an organic radical generated by an iron-sulphur enzyme. *Nature* **465**, 891–896 (2010). doi:10.1038/nature09138

6. M. Dong, X. Su, B. Dzikovski, E. E. Dando, X. Zhu, J. Du, J. H. Freed, H. Lin, Dph3 is an electron donor for Dph1-Dph2 in the first step of eukaryotic diphthamide biosynthesis. *J. Am. Chem. Soc.* **136**, 1754–1757 (2014). doi:10.1021/ja4118957 Medline

7. M. Dong, M. Horitani, B. Dzikovski, M.-E. Pandelia, C. Krebs, J. H. Freed, B. M. Hoffman, H. Lin, Organometallic complex formed by an unconventional radical S-adenosylmethionine enzyme. *J. Am. Chem. Soc.* **138**, 9755–9758 (2016). doi:10.1021/jacs.6b04155 Medline

8. J. B. Broderick, B. R. Duffus, K. S. Duschene, E. M. Shepard, Radical S-adenosylmethionine enzymes. *Chem. Rev.* **114**, 4229–4317 (2014). doi:10.1021/cr4004709 Medline

9. M. Horitani, K. Shisler, W. E. Broderick, R. U. Hutcheson, K. S. Duschene, A. R. Marts, B. M. Hoffman, J. B. Broderick, Radical SAM catalysis via an organometallic intermediate with an Fe-[5′-C]-deoxyadenosyl bond. *Science* **352**, 822–825 (2016). doi:10.1126/science.aaf5327 Medline

10. G. E. Cutsail 3rd, J. Telser, B. M. Hoffman, Advanced paramagnetic resonance spectroscopies of iron-sulfur proteins: Electron nuclear double resonance (ENDOR) and electron spin echo envelope modulation (ESEEM). *Biochim. Biophys. Acta* **1853**, 1370–1394 (2015). doi:10.1016/j.bbamcr.2015.01.025 Medline

11. A. Carrington, A. D. McLachlan, *Introduction to Magnetic Resonance with Applications to Chemistry and Chemical Physics* (Harper & Row, New York, 1967)

12. M. Dong, M. Horitani, B. Dzikovski, J. H. Freed, S. E. Ealick, B. M. Hoffman, H. Lin, Substrate-dependent cleavage site selection by unconventional radical S-adenosylmethionine enzymes in diphthamide biosynthesis. *J. Am. Chem. Soc.* **139**, 5680–5683 (2017). doi:10.1021/jacs.7b01712 Medline

13. J. L. Vey, J. Yang, M. Li, W. E. Broderick, J. B. Broderick, C. L. Drennan, Structural asis for glycyl radical formation by pyruvate formate-lyase activating enzyme. *Proc. Natl. Acad. Sci. U.S.A.* **105**, 16137–16141 (2008). doi:10.1073/pnas.0806640105 Medline

14. J. A. Kampmeier, Regioselectivity in the homolytic cleavage of S-adenosylmethionine. *Biochemistry* **49**, 10770–10772 (2010). doi:10.1021/bi101509u Medline

15. J. Frazzon, D. R. Dean, Formation of iron-sulfur clusters in bacteria: An emerging field in bioinorganic chemistry. *Curr. Opin. Chem. Biol.* **7**, 166–173 (2003). doi:10.1016/S1367-5931(03)00021-8 Medline

16. H. Beinert, Semi-micro methods for analysis of labile sulfide and of labile sulfide plus sulfane sulfur in unusually stable iron-sulfur proteins. *Anal. Biochem.* **131**, 373–378 (1983). doi:10.1016/0003-2697(83)90186-0 Medline

17. X. Su, W. Chen, W. Lee, H. Jiang, S. Zhang, H. Lin, YBR246W is required for the third step of diphthamide biosynthesis. *J. Am. Chem. Soc.* **134**, 773–776 (2012). doi:10.1021/ja208870a Medline

18. J. Du, H. Jiang, H. Lin, Investigating the ADP-ribosyltransferase activity of sirtuins with NAD analogues and 32P-NAD. *Biochemistry* **48**, 2878–2890 (2009). doi:10.1021/bi802093g Medline

19. R. Wang, W. Zheng, M. Luo, A sensitive mass spectrum assay to characterize engineered methionine adenosyltransferases with S-alkyl methionine analogues as substrates. *Anal. Biochem.* **450**, 11–19 (2014). doi:10.1016/j.ab.2013.12.026 Medline

20. J. D. Caranto, A. C. Vilbert, K. M. Lancaster, *Nitrosomonas europaea* cytochrome P460 is a direct link between nitrification and nitrous oxide emission. *Proc. Natl. Acad. Sci. U.S.A.* **113**, 14704–14709 (2016). doi:10.1073/pnas.1611051113 Medline

21. M. M. Werst, C. E. Davoust, B. M. Hoffman, Ligand spin densities in blue copper proteins by q-band proton and nitrogen-14 ENDOR spectroscopy. *J. Am. Chem. Soc.* **113**, 1533–1538 (1991). doi:10.1021/ja00005a011

22. C. E. D. Davoust, P. E. Doan, B. M. Hoffman, Q-band pulsed electron spin-echo spectrometer and its application to ENDOR and ESEEM. *J. Magn. Reson. A* **119**, 38–44 (1996). doi:10.1006/jmra.1996.0049

23. Z. Otwinowski, W. Minor, Processing of x-ray diffraction data collected in oscillation mode. *Methods Enzymol.* **276**, 307–326 (1997). doi:10.1016/S0076-6879(97)76066-X

24. P. D. Adams, P. V. Afonine, G. Bunkóczi, V. B. Chen, I. W. Davis, N. Echols, J. J. Headd, L.-W. Hung, G. J. Kapral, R. W. Grosse-Kunstleve, A. J. McCoy, N. W. Moriarty, R. Oeffner, R. J. Read, D. C. Richardson, J. S. Richardson, T. C. Terwilliger, P. H. Zwart, PHENIX: A comprehensive Python-based system for macromolecular structure solution. *Acta Crystallogr. D Biol. Crystallogr.* **66**, 213–221 (2010). doi:10.1107/S0907444909052925 Medline

25. P. Emsley, B. Lohkamp, W. G. Scott, K. Cowtan, Features and development of Coot. *Acta Crystallogr. D Biol. Crystallogr.* **66**, 486–501 (2010). doi:10.1107/S0907444910007493 Medline

26. J. Painter, E. A. Merritt, Optimal description of a protein structure in terms of multiple groups undergoing TLS motion. *Acta Crystallogr. D Biol. Crystallogr.* **62**, 439–450 (2006). doi:10.1107/S0907444906005270 Medline

27. V. B. Chen, W. B. Arendall 3rd, J. J. Headd, D. A. Keedy, R. M. Immormino, G. J. Kapral, L. W. Murray, J. S. Richardson, D. C. Richardson, MolProbity: All-atom structure validation for macromolecular crystallography. *Acta Crystallogr. D Biol. Crystallogr.* **66**, 12–21 (2010). doi:10.1107/S0907444909042073 Medline

28. M. K. Fenwick, A. P. Mehta, Y. Zhang, S. H. Abdelwahed, T. P. Begley, S. E. Ealick, Non-canonical active site architecture of the radical SAM thiamin pyrimidine synthase. *Nat. Commun.* **6**, 6480 (2015). doi:10.1038/ncomms7480 Medline

29. A. P. Mehta, S. H. Abdelwahed, M. K. Fenwick, A. B. Hazra, M. E. Taga, Y. Zhang, S. E. Ealick, T. P. Begley, Anaerobic 5-hydroxybenzimidazole formation from aminoimidazole ribotide: an unanticipated intersection of thiamin and vitamin B_{12} Biosynthesis. *J. Am. Chem. Soc.* **137**, 10444–10447 (2015). doi:10.1021/jacs.5b03576 Medline

30. M. K. Fenwick, Y. Li, P. Cresswell, Y. Modis, S. E. Ealick, Structural studies of viperin, an antiviral radical SAM enzyme. *Proc. Natl. Acad. Sci. U.S.A.* **114**, 6806–6811 (2017). Medline

31. P. Hänzelmann, H. L. Hernández, C. Menzel, R. García-Serres, B. H. Huynh, M. K. Johnson, R. R. Mendel, H. Schindelin, Characterization of MOCS1A, an oxygen-sensitive iron-sulfur protein involved in human molybdenum cofactor biosynthesis. *J. Biol. Chem.* **279**, 34721–34732 (2004). doi:10.1074/jbc.M313398200 Medline

32. A. P. Mehta, J. W. Hanes, S. H. Abdelwahed, D. G. Hilmey, P. Hänzelmann, T. P. Begley, Catalysis of a new ribose carbon-insertion reaction by the molybdenum cofactor biosynthetic enzyme MoaA. *Biochemistry* **52**, 1134–1136 (2013). doi:10.1021/bi3016026 Medline

33. A. J. McCoy, R. W. Grosse-Kunstleve, P. D. Adams, M. D. Winn, L. C. Storoni, R. J. Read, Phaser crystallographic software. *J. Appl. Crystallogr.* **40**, 658–674 (2007). doi:10.1107/S0021889807021206 Medline

34. T. L. Grove, J. Livada, E. L. Schwalm, M. T. Green, S. J. Booker, A. Silakov, A substrate radical intermediate in catalysis by the antibiotic resistance protein Cfr. *Nat. Chem. Biol.* **9**, 422–427 (2013). doi:10.1038/nchembio.1251 Medline

35. A. Silakov, T. L. Grove, M. I. Radle, M. R. Bauerle, M. T. Green, A. C. Rosenzweig, A. K. Boal, S. J. Booker, Characterization of a cross-linked protein-nucleic acid substrate radical in the reaction catalyzed by RlmN. *J. Am. Chem. Soc.* **136**, 8221–8228 (2014). doi:10.1021/ja410560p Medline